Determination of the anisotropies and reversal process in exchange-bias bilayers using a rotational magnetization curve approach

Wenbo Sui, Jingyi Zhu, Jinyun Li, Guozhi Chai, Changjun Jiang, Xiaolong Fan, and Desheng Xue[a)]
Key Laboratory for Magnetism and Magnetic Materials of the MOE, Lanzhou University, Lanzhou 730000, People's Republic of China

(Received 13 January 2011; accepted 29 March 2011; published online 17 May 2011)

Rotational magnetization curves of the exchange-bias bilayers were investigated based on the Stoner-Wohlfarth model, which can be grouped into three cases according to the magnetization reversal process. The unidirectional anisotropic field $H_E = 41.4$ Oe, the uniaxial anisotropic field $H_k = 4.2$ Oe and the accurate direction of the easy axis of our FeNi/FeMn exchange-bias bilayers were obtained by fitting their experimental rotational magnetization curves. During the rotational process the magnetization reversal of the bilayers is a coherent rotation with a critical magnetization reversal field $H_1 = 41.372$ Oe. © *2011 American Institute of Physics*. [doi:10.1063/1.3583664]

I. INTRODUCTION

Exchange bias (EB) discovered in fine particle of cobalt with a cobaltous oxide shell is known as a phenomenon in which the hysteresis loop is shifted along the magnetic field axis in ferromagnet (FM)/antiferromagnet bilayers.[1,2] The EB effect has been also found in FM/ferrimagnet core-shell particles,[3] soft FM/hard FM bilayers[4] and FM/sperimagnetic rare earth transition-metal amorphous alloys trilayers.[5] It is the EB effect results in new performance of devices, such as magnetoresistive sensors,[6–10] magnetic sensors,[11–16] and read-heads.[16–18] Meanwhile, both training effect[19–21] and spin-transfer effect[22] are also observed in the EB system. All of the effects are both closely related to the unidirectional anisotropic field H_E which is from the interfacial exchange coupling and the uniaxial anisotropic field H_k which is from the FM layer. However, how to determine quantitatively H_E and H_k of the EB system is a challenge for the EB fundamental research and application.

Many experimental techniques have been used to investigate the anisotropy of the EB bilayers. The hysteresis loops method is commonly used, which can be realized with superconducting quantum interference device magnetometer,[23–25] vibrating sample magnetometer (VSM),[25,26] magneto-optical Kerr effect (MOKE),[27–30] and loop tracers.[31,32] Only H_E can be derived directly from the shift of the hysteresis loops. Dynamic measurements by using ferromagnetic resonance spectrometer,[33] pulsed inductive microwave magnetometer,[34] and vector network analyzer[35] are employed to obtain indirectly the effective anisotropic field rather than H_E and H_k from resonance frequency. As the anisotropic fields are closely related to the magnetization and reversal mechanism, a way that the coherent rotation can be achieved is more effective for extracting accurately H_E and H_k in the EB system.

By fitting the hard axis loop[36,37] and using the torque method,[38,39] the rotating magnetic field MOKE technique,[40–42] and the rotational magnetization curve,[43] both H_E and H_k in the EB bilayers should be obtained. Meanwhile, the magnetization reversal process can be studied. Actually, the hard axis loop gives us a good approximation of H_k, the torque method reveals the saturation magnetization reversal process, the so-called rotating magnetic field MOKE technique reveals the magnetization reversal process of the light-spot position of the sample, and the rotational magnetization curve reveals the magnetization reversal process of the whole of the sample at any external field H.

In this paper, the rotational magnetization curve, as a typical direct measurement for anisotropy, was used to investigate H_k and H_E as well as the magnetization reversal process in the EB system. By fitting the experimental results of the FeNi/FeMn bilayers with the theoretical equation, the accurate values of the two anisotropic fields and the magnetization reversal process at different H were obtained. At the same time, the accurate direction of the easy axis (EA) and the hard axis (HA) can be derived.

II. THEORETICAL MODEL

Supposing the saturation magnetization $\mathbf{M}_s$ of the EB bilayers lies in the film plane, the in-plane rotation of $\mathbf{M}_s$ under an external field $\mathbf{H}$ applied in film plane is satisfied with a coherent rotation as shown in Fig. 1(a). According to the Stoner-Wohlfarth (SW) model,[44] the total effective energy density of the EB bilayers can be written as[2,30]

$$F = -K_E \cos\theta + K_1 \sin^2\theta - \mu_0 M_s H \cos(\theta_0 - \theta).$$

In order to make the unidirectional and uniaxial anisotropic energy densities have the same zero-potential-energy reference surface, we make a simple transformation

$$\cos\theta = 1 - 2\sin^2\frac{\theta}{2},$$

then the total effective energy density can be rewritten as

[a)]Electronic mail: xueds@lzu.edu.cn.

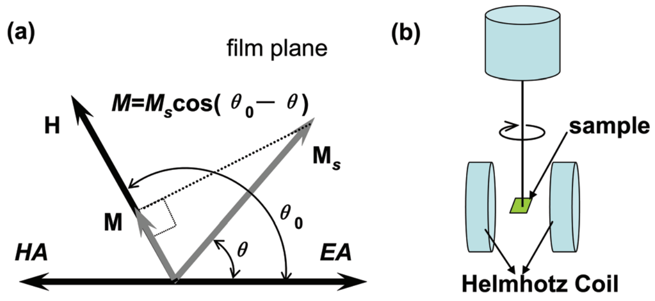

FIG. 1. (Color online) (a) Definition of axes and angles of the EB bilayers during the in-plane rotation of an external field **H**; (b) Schematic drawing of equipment structure of a commercial VSM. EA is anti-parallel to HA for the EB bilayers.

$$F = K_0 + K_E \sin^2\frac{\theta}{2} + K_1 \sin^2\theta - \mu_0 M_s H \cos(\theta_0 - \theta), \quad (1)$$

where K_0 is a constant, K_E is the unidirectional anisotropic constant, K_1 is the uniaxial anisotropic constant, θ_0 (θ) is the angle between the direction of EA and **H** ($\mathbf{M}_s$). An equilibrium state of $\mathbf{M}_s$ is one which minimized Eq. (1).

With the definition of the unidirectional and the uniaxial anisotropic field H_E and H_k

$$H_E = \frac{K_E}{2\mu_0 M_s}, \quad H_k = \frac{2K_1}{\mu_0 M_s}, \quad (2)$$

the optimization problem is more conveniently stated in terms of reduced quantities, $h = H/H_k$, $m = H_E/H_k$, $f = F/K_1$ and supposed $K_0 = 0$. The equilibrium position θ of M_s at different reduced fields h is one which minimizes

$$f = 4m\sin^2\frac{\theta}{2} + \sin^2\theta - 2h\cos(\theta_0 - \theta), \quad (3)$$

subject to the conditions

$$\partial f/\partial\theta = 0, \quad (4)$$

$$\partial^2 f/\partial\theta^2 > 0. \quad (5)$$

When the EB bilayers is rotated in VSM as shown in Fig. 1(b), the rotational magnetization curve is achieved as the θ_0 dependence of the magnetization M which is satisfied with

$$M = M_s\cos(\theta_0 - \theta). \quad (6)$$

With the increase of h, the rotation of $\mathbf{M}_s$ may undergo different cases of the magnetization reversal process, the transition from one case to others can be determined by

$$\partial f/\partial\theta = 0, \ \partial^2 f/\partial\theta^2 = 0, \quad (7)$$

and yields

$$\begin{aligned} h_1 &= \frac{1}{8}\sqrt{2(8 + 20m^2 - m^4 + (m^3 + 8m)\sqrt{m^2+8})}, \\ h_2 &= \sqrt{m^2+1}, \end{aligned} \quad (8)$$

where h_1 and h_2 are the critical reduced fields of transition.

Because $h_1 < h_2$, for any value of m corresponding to different EB bilayers the rotational magnetization curve can be divided into three cases: $0 \le h < h_1$, $h_1 < h < h_2$ and $h > h_2$. Obviously, the magnitude of h determines the different magnetization reversal process of the sample. It is worth investigating the characteristics of these three cases of the magnetization reversal process with any value of m.

III. CASES OF ROTATIONAL MAGNETIZATION CURVES

Supposing $m = 1.1$, $h_1 = 1.386$ and $h_2 = 1.487$ can be obtained from Eq. (8). Combining the rotational magnetization curve with the $\theta \sim \theta_0$ and $f \sim \theta_0$ curves, each case of the magnetization reversal process is investigated.

A. Case 1. Nonreversed magnetization rotating process with $0 \le h < h_1$

Figure 2 shows the $\theta \sim \theta_0$ curves and the rotational magnetization curves, which are both continuous with a period of 2π. As shown in Fig. 2(a), when $h = 0$, θ is entirely quiet. With the increase of h, the change of θ becomes more and more significant. With Eq. (4), the largest value of θ at h_1 satisfies

$$(m + \cos\theta)\sin\theta = h_1, \quad (9)$$

while the torque from the external field is the largest and equals $\mu_0\mathbf{M}_s\mathbf{H}$. It is found that the maximum angle of $\mathbf{M}_s$ deviating from EA cannot be larger than 90°. Therefore, in $0 \le h < h_1$, $\mathbf{M}_s$ cannot be reversed. From the $M/\mathbf{M}_s \sim \theta_0$

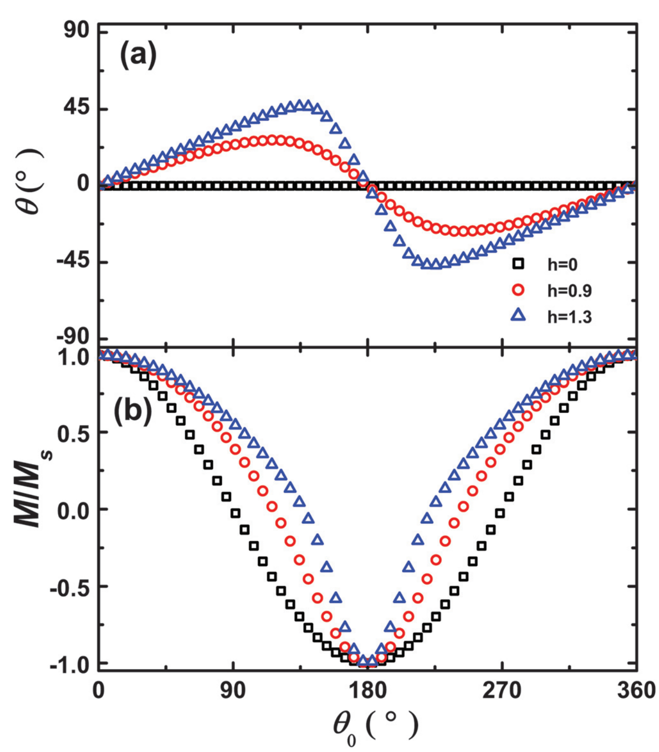

FIG. 2. (Color online) (a) The equilibrium position of $\mathbf{M}_s$ θ and (b) the normalized magnetization $M/\mathbf{M}_s$ as a function of θ_0 at $h = 0$, 0.9, and 1.3. $\theta_0 = 0(180)^\circ$ represents the direction where **H** is parallel to EA (HA).

curves shown in Fig. 2(b), it is found that when $h = 0$, $\mathbf{M}_s$ is stable at EA, and $M/\mathbf{M}_s$ equals $\cos\theta_0$. The rotational magnetization curve becomes narrower as the value of h increases until the discontinuous magnetic rotation occurs at $h = h_1$. With Eq. (6), $M/\mathbf{M}_s < 0$ suggests the angle $|\theta_0 - \theta|$ between $\mathbf{H}$ and $\mathbf{M}_s$ is greater than 90°, which also means that $\mathbf{M}_s$ is not reversed. For any coherent EB bilayers, there is only one direction of EA. When $\mathbf{H}$ is parallel to EA, the value of magnetization, the horizontal component of $\mathbf{M}_s$ at the direction of $\mathbf{H}$, is the maximum value and equals to M_s, so we can obtain the direction of EA from the position of the maximum value on the rotational magnetization curve. In this case, $\theta_0 = 0(180)^\circ$ represents the direction where $\mathbf{H}$ is parallel to EA (HA).

B. Case 2. Discontinuous magnetization reversal process with $h_1 < h < h_2$

Figure 3 shows the $\theta \sim \theta_0$ curves and the rotational magnetization curves which become discontinuous with a period of 2π. As shown in Fig. 3(a), two "jumps" emerge at $\theta_0 \approx 140^\circ$ and 220°, respectively. These two discontinuous "jumps" correspond to the magnetization reversal: EA $\rightarrow$ HA or HA $\rightarrow$ EA. Related "jumps"occur in the $M/\mathbf{M}_s \sim \theta_0$ curves shown in Fig. 3(b). The values of $M/\mathbf{M}_s$ are consistently greater than zero, which means that the maximum angle between $\mathbf{H}$ and $\mathbf{M}_s$ is less than 90° during the rotation. In order to get an insight into the magnetization reversal process, f as a function of θ is further investigated near the "jumps" point of the magnetization reversal.

Figure 4 shows the $f \sim \theta$ curves at $h = 1.45$ for three θ_0. When $\theta_0 = 139.3^\circ$, there are two energy minima marked as

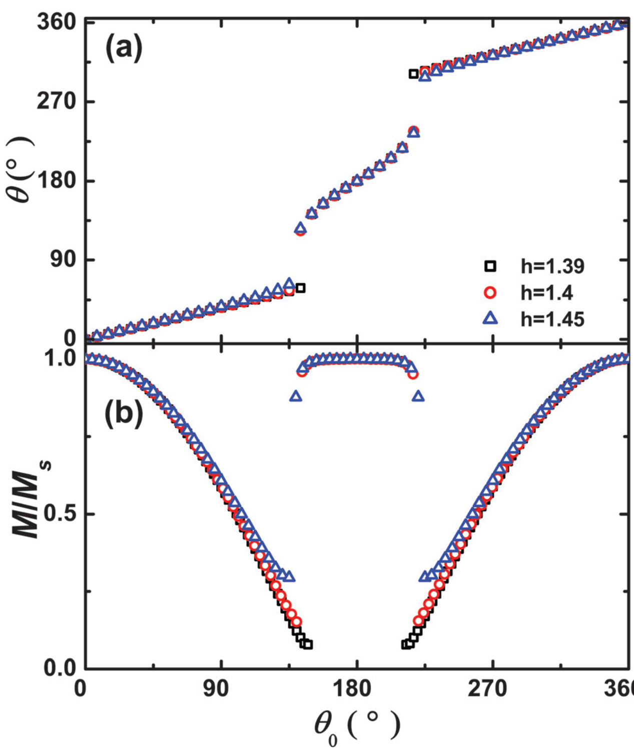

FIG. 3. (Color online) (a) The equilibrium position of $\mathbf{M}_s$ θ and (b) the normalized magnetization $M/\mathbf{M}_s$ as a function of θ_0 at $h = 1.39$, 1.4, and 1.45.

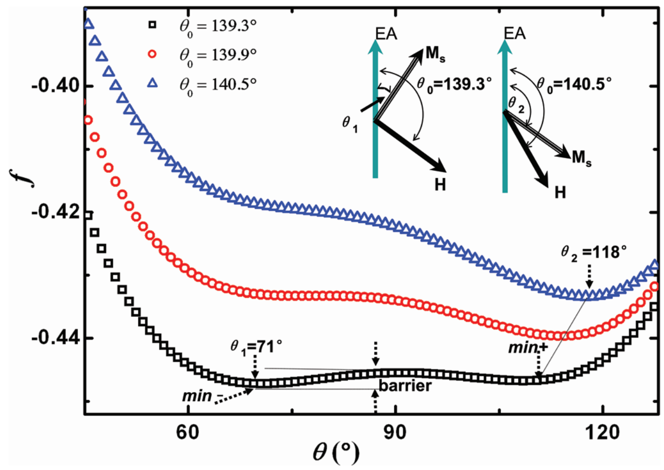

FIG. 4. (Color online) The θ dependence of reduced f at $h = 1.45$ for $\theta_0 = 139.3^\circ$, 139.9°, and 140.5°. The insets schematically show the magnetization states before and after the magnetization reversal.

min $-$ and min $+$ with a barrier between them, and the equilibrium position of $\mathbf{M}_s$ stays at min $-$. With the increase of θ_0, the barrier disappears, in turn, the equilibrium state of $\mathbf{M}_s$ changes from min $-$ to min $+$, which means the magnetization is reversed. The magnetization reversal occurs at $\theta_0 \approx 139.9^\circ$, which corresponds to the critical point of the discontinuous magnetization reversal process. The insets schematically show the positions of $\mathbf{M}_s$ before and after the magnetization reversal for $\theta_0 = 139.3^\circ$ and 140.5°, respectively. It is found that nearby the critical point, any tiny switch of the direction of the external field can trigger an enormous change of $\mathbf{M}_s$.

C. Case 3. Continuous magnetization reversal process with $h > h_2$

Figure 5 shows that both $\theta \sim \theta_0$ curves and the rotational magnetization curves are continuous, and the discontinuous phenomena of θ vanish at $\theta = 90^\circ$. As the value of h increases, the curves become smooth, which means the larger the field H, the nearer the direction of $\mathbf{M}_s$ close to it. This indicates that when the external filed is strong enough to conquer the interfacial exchange-coupling interaction and the ferromagnetic anisotropy, the magnetization rotating process is a continuous magnetization reversal process.

Figure 6 shows the θ dependence of f at $h = 2$. There is only one minimum and no barrier on each curve. It is found that the minima of the $f \sim \theta_0$ curves appear at $\theta = 82.3^\circ$, 90°, and 99.6° when $\theta_0 = 120^\circ$, 123.5°, and 127°, respectively. The equilibrium position of $\mathbf{M}_s$ can be stable at $\theta = 90^\circ$, which reveals that the magnetization reversal process becomes continuous in this case. The insets schematically show the positions of $\mathbf{M}_s$ for $\theta_0 = 120^\circ$, 123.5°, and 127°, respectively, where $\theta_0 = 123.5^\circ$ is the critical point of the magnetization reversal.

IV. EXPERIMENTAL RESULTS AND DISCUSSION

The sample FeNi (6 nm)/FeMn (10 nm) with a Ta (2 nm) buffer layer and a Ta (2 nm) cover layer was deposited on Si(100) substrate by magnetron sputtering system using

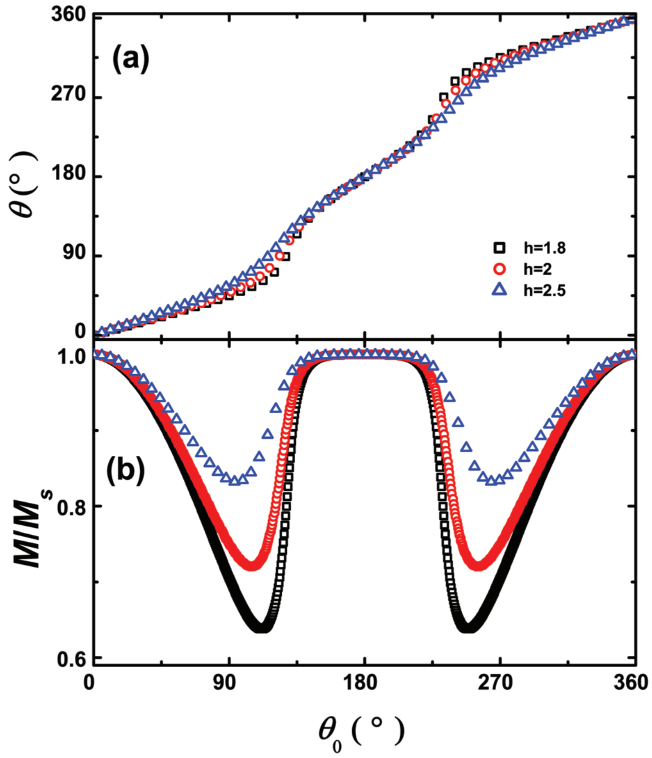

FIG. 5. (Color online) (a) The equilibrium position of M_s θ and (b) the normalized magnetization $M/\mathbf{M}_s$ as a function of θ_0 at $h = 1.8$, 2, and 2.5.

targets of $Fe_{19}Ni_{81}$, $Fe_{50}Mn_{50}$, and Ta. The base pressure and Ar pressure during deposition were 3.0×10^{-7} Torr and 2 mTorr. A permanent magnetic field of 120 Oe was applied parallel to the film plane during the deposition to develop a necessary exchange bias. No further field annealing and cooling procedures were carried out.

Figure 7 shows the rotational magnetization curves of the EB sample FeNi (6 nm)/FeMn (10 nm) measured at room temperature with VSM for $H = 20$, 35, and 60 Oe. It is found that all of three curves are continuous, the curves for $H = 20$, 35 Oe (60 Oe) are similar to the *Case 1*[3] of the theoretical rotational magnetization curves. As the magnetization reversal mechanism of the sample is a coherent rotation

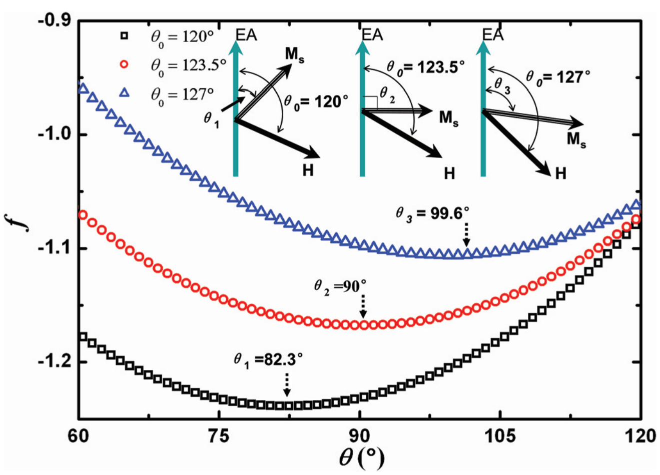

FIG. 6. (Color online) The θ dependence of reduced f at $h = 2$ for $\theta_0 = 120°$, 123.5°, and 127°. The insets schematically show the magnetization states before, at, and after the magnetization reversal.

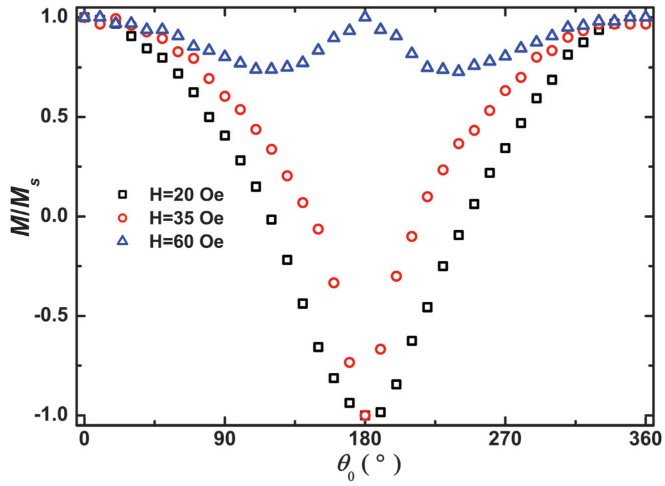

FIG. 7. (Color online) Experimental results of FeNi/FeMn sample at $H = 20$, 35, and 60 Oe. $\theta_0 = 180°$ represents the direction where $\mathbf{H}$ is parallel to HA.

during the in-plane rotational magnetization, the direction of EA (HA) exists at $\theta_0 = 0(180)^\circ$ comparing with *Case 1* of the theoretical rotational magnetization curve.

In principle, the anisotropic fields H_E and H_k of the EB bilayers can be obtained by fitting the experimental rotational magnetization curve with Eq. (6). Actually, it is convenient to transform the rotational magnetization curve into $\sin(\theta_0 - \theta)$ as a function of θ at different H. From the equilibrium condition Eq. (4), $\sin(\theta_0 - \theta)$ as a function of θ is

$$\frac{H_E}{H}\sin\theta + \frac{H_k}{2H}\sin 2\theta = \sin(\theta_0 - \theta). \qquad (10)$$

The value of θ is synchronously satisfied with the both sides of Eq. (10). Defining

$$g(\theta) \equiv \frac{H_E}{H}\sin\theta + \frac{H_k}{2H}\sin 2\theta, \qquad (11)$$

the values of $H_E = 41.4$ Oe, $H_k = 4.2$ Oe, and $m = 9.8$ of the EB bilayers can be obtained by fitting the experimental $\sin(\theta - \theta_0)$ curves with Eq. (11). As shown in Fig. 8, the

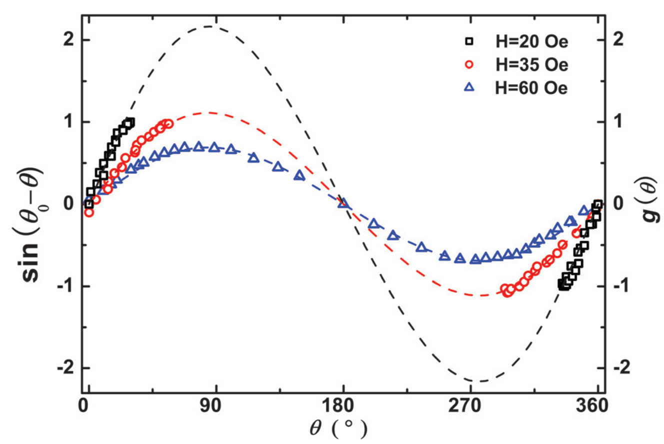

FIG. 8. (Color online) The symbols (squares, circles, and triangles) are the experimental $\sin(\theta_0 - \theta)$ as a function of θ deduced from the rotational magnetization curves of the FeNi/FeMn EB bilayers at $H = 20$, 35, and 60 Oe, respectively. The dash lines are the $g(\theta)$as a function of θ fitted by Eq. (11).

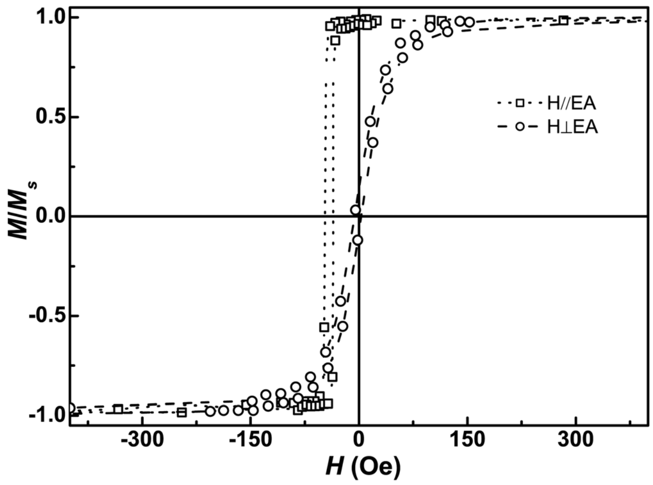

FIG. 9. Normalized magnetic hysteresis loops measured at room temperature with **H** parallel and perpendicular to EA determined by the experimental rotational magnetization curves.

symbols (squares, circles, and triangles) show $\sin(\theta - \theta_0)$ as a function of θ corresponding to three deferent H, and the dash lines are the curves fitted with Eq. (11).

In order to verify the above results, Fig. 9 shows the normalized magnetic hysteresis loops at **H** parallel and perpendicular to the direction of EA determined by the experimental rotational magnetization curve. $H_E = 40.4$ Oe, obtained from the hysteresis loops, is close to the value obtained above (41.4 Oe). It is believed that the rotational magnetization curve approach is still effective to obtain the values of H_k.[43]

According to $m = 9.8$ and $H_k = 4.2$ Oe, we can obtain the critical reduced fields $h_1 = 9.850$ and $h_2 = 9.851$, from which the corresponding critical fileds $H_1 = 41.372$ Oe and $H_2 = 41.374$ Oe are derived for our sample FeNi (6 nm)/FeMn (10 nm). Theoretically, we can obtain the magnetization reversal angle $\theta_0 = 173.75°$ and $\theta_0 = 174.35°$ at H_1 and H_2, respectively. It is clearly found that in *Case 2*, the range of H is only 0.02 Oe and the range of the corresponding magnetization reversal angle is only 0.6°, which are so small that the *Case 2* cannot be observed experimentally.

V. CONCLUSION

Based on the SW model, we investigate the theoretical and experimental rotational magnetization curves of the EB bilayers. For the EB bilayers, the magnetization reversal process includes three cases: nonreversed magnetization rotating process, discontinuous magnetization reversal process and continuous magnetization reversal process. The direction of EA of the EB bilayers can be determined by the maxima of $M/\mathbf{M}_s$ occurred in *Case 1*. For the nonlinear EB bilayers,[45,46] the rotational magnetization curve approach is still effective, which can help us obtain the direction of EA. The experimental rotational magnetization curve indicates that the magnetization reversal mechanism of the sample FeNi (6 nm)/FeMn (10 nm) is a coherent rotation. The anisotropic fields $H_E = 41.4$ Oe and $H_k = 4.2$ Oe of the sample are acquired by fitting experimental $\sin(\theta - \theta_0)$ with Eq. (11) without knowing the direction of EA before measurement. Combing the experimental results with the theoretical calculations, we obtain the critical magnetization reversal field ($H_1 = 41.372$ Oe) of the EB bilayers. For our sample, the ranges of H and the corresponding magnetization reversal angle in the discontinuous magnetization reversal process are too small to be observed experimentally.

ACKNOWLEDGMENTS

This work is supported by National Natural Science Foundation of China (Grant No. 10774062), National Nature Science Foundation of China (Grant No.50902064), National Science Fund for Distinguished Young Scholars (Grant No. 50925103), and the Key grant Project of Chinese Ministry of Education (Grant No. 309027).

[1]W. H. Meiklejohn and C. P. Bean, Phys. Rev. **102**, 1413 (1956).
[2]M. Vasilakaki and K. N. Trohidou, Phys. Rev. B **79**, 144402 (2009).
[3]C. Binek, S. Polisetty, X. He, and A. Berger, Phys. Rev. Lett. **96**, 067201 (2006).
[4]F. Csikor, Z. Fodor, and J. Heitger, Phys. Rev. Lett. **82**, 21 (1999).
[5]J. Nogués and I. K. Schuller, J. Magn. Magn. Mater. **192**, 203 (1999).
[6]B. Dieny, V. S. Speriosu, S. S. P. Parkin, B. A. Gurney, D. R. Wilhoit, and D. Mauri, Phys. Rev. B **43**, 1297 (1991).
[7]L. V. Melo, L. M. Rodrigues, and P. P. Freitas, IEEE Trans. Magn. **33**, 3295 (1997).
[8]K. Matsuyama, H. Asada, S. Ikeda, and K. Taniguchi, IEEE Trans. Magn. **33**, 3283 (1997).
[9]D. D. Tang, P. K. Wang, V. S. Speriosu, S. Le, and K. K. Kung, IEEE Trans. Magn. **31**, 3206 (1995).
[10]T. Lin, C. Tsang, R. E. Fontana, and J. K. Howard, IEEE Trans. Magn. **31**, 2584 (1995).
[11]N. Smith, A. M. Zeltser, D. L. Yang, and P. V. Koeppe, IEEE Trans. Magn. **33**, 3385 (1997).
[12]J. L. Leal, N. J. Oliveira, L. M. Rodrigues, A. T. Sousa, and P. P. Freitas, IEEE Trans. Magn. **30**, 3831 (1994).
[13]P. P. Freitas, J. L. Leal, L. V. Melo, N. J. Oliveira, L. Rodrigues, and A. T. Sousa, Appl. Phys. Lett. **65**, 493 (1994).
[14]M. M. Miller, P. Lubitz, G. A. Prinz, J. J. Krebs, A. S. Edelstein, S. F. Cheng, and F. G. Parsons, IEEE Trans. Magn **33**, 3388 (1997).
[15]K. M. H. Lenssen, A. E. M. D. Vierman, and J. J. T. M. Donkers, J. Appl. Phys. **81**, 4915 (1997).
[16]J. Fujikata, K. Ishihara, K. Hayashi, H. Yamamoto, and K. Yamada, IEEE Trans. Magn. **31**, 3936 (1995).
[17]H. Yoda, H. Iwasaki, T. Kobayashi, A. Tsutai, and M. Sahashi, IEEE Trans. Magn. **32**, 3363 (1996).
[18]N. J. Oliveira, J. L. Ferreira, J. Pinheiro, A. M. Fernandes, O. Redon, S. X. Li, P. ten Berge, T. S. Plaskett, and P. P. Freitas, J. Appl. Phys. **81**, 4903 (1997).
[19]D. Paccard, C. Schlenker, O. Massenet, R. Montmory, and A. Yelon, Phys. Status Solidi. **16**, 301 (1966).
[20]L. Fernandez-Outon, G. Vallejo-Fernandez, S. Manzoor, and K. O'Grady, J. Magn. Magn. Mater. **303**, 296 (2006).
[21]A. G. Biternas, U. Nowak, and R. W. Chantrell, Phys. Rev. B **80**, 134419 (2009).
[22]X. L. Tang, H. W. Zhang, H. Su, Y. L. Jing, and Z. Y. Zhong, Phys. Rev. B **81**, 052401 (2010).
[23]K. Olejnik, P. Wadley, J. A. Haigh, K. W. Edmonds, R. P. Campion, A. W. Rushforth, B. L. Gallagher, C. T. Foxon, T. Jungwirth, J. Wunderlich, S. S. Dhesi, S. A. Cavill, G. van der Laan, and E. Arenholz, Phys. Rev. B **81**, 104402 (2010).
[24]T. J. Moran, J. M. Gallego, and I. K. Schuller, J. Appl. Phys. **78**, 1887 (1995).
[25]Y. Suzuki, R. B. van Dover, E. M. Gyorgy, J. M. Phillips, V. Korenivski, D. J. Werder, C. H. Chen, R. J. Felder, R. J. Cava, J. J. Krajewski, and J. W. F. Peck, J. Appl. Phys. **79**, 5923 (1996).
[26]C. Schlenker, S. S. P. Parkin, J. C. Scott, and K. Howard, J. Magn. Magn. Mater. **54**, 801 (1986).
[27]R. Jungblut, R. Coehoorn, M. T. Johnson, J. aan de Stegge, and A. Reinders, J. Appl. Phys. **75**, 6659 (1994).

[28]W. C. Cain and M. H. Kryder, J. Appl. Phys. **67**, 5722 (1990).
[29]A. Berger and H. Hopster, Phys. Rev. Lett. **73**, 193 (1994).
[30]M. A. Russak, S. M. Rossnagel, S. L. Cohen, T. McGuire, G. J. Scilla, C. V. Jahnes, J. M. Baker, and J. J. Cuomo, J. Electrochem Soc. **136**, 1793 (1989).
[31]T. Tokunaga, M. Taguchi, T. Fukami, Y. Nakaki, and K. Tsutsumi, J. Appl. Phys. **67**, 4417 (1990).
[32]T. J. Klemmer, V. R. Inturi, M. K. Minor, and J. A. Barnard, Appl. Phys. Lett. **70**, 2915 (1997).
[33]A. Layadi, J. W. Lee, and J. O. Artman, J. Appl. Phys. **63**, 3808 (1988).
[34]M. L. Schneider, A. B. Kos, and T. J. Silva, Appl. Phys. Lett. **86**, 202503 (2005).
[35]C. J. Jiang, D. S. Xue, D. W. Guo, and X. L. Fan, J. Appl. Phys. **106**, 103910 (2009).
[36]M. Grimsditch, A. Hoffmann, P. Vavassori, H. Shi, and D. Lederman, Phys. Rev. Lett. **90**, 257201 (2003).
[37]J. Camarero, J. Sort, A. Hoffmann, J. M. García-Martín, B. Dieny, R. Miranda, and J. Nogués, Phys. Rev. Lett. **95**, 057204 (2005).
[38]A. E. Berkowitz and J. H. Greiner, J. Appl. Phys. **36**, 3330 (1965).
[39]J. Bransky, I. Bransky, and A. A. Hirsch, J. Appl. Phys. **41**, 183 (1970).
[40]D. Berling, S. Zabrocki, R. Stephan, G. Garreau, J. L. Bubendorff, A. Mehdaoui, D. Bolmont, P. Wetzel, C. Pirri, and G. Gewinner, J. Magn. Magn. Mater. **297**, 118 (2006).
[41]Z. Tian, C. S. Tian, L. F. Yin, D. Wu, G. S. Dong, X. Jin, and Z. Q. Qiu, Phys. Rev. B **70**, 012301 (2004).
[42]C. S. Tian, D. Qian, D. Wu, R. H. He, Y. Z. Wu, W. X. Tang, L. F. Yin, Y. S. Shi, G. S. Dong, X. F. Jin, X. M. Jiang, F. Q. Liu, H. J. Qian, K. Sun, L. M. Wang, G. Rossi, Z. Q. Qiu, and J. Shi, Phys. Rev. Lett. **94**, 137210 (2005).
[43]D. S. Xue, X. L. Fan, and C. J. Jiang, Appl. Phys. Lett. **89**, 011910 (2006).
[44]E. C. Stoner and E. P. Wohlfarth, Phil. Trans. R. Soc. Lond. A **240**, 599 (1948).
[45]E. Jiménez, J. Camarero, J. Sort, J. Nogués, N. Mikuszeit, J. M. García-Martín, A. Hoffmann, B. Dieny, and R. Miranda, Phys. Rev. B **80**, 014415 (2009).
[46]J. McCord, C. Hamann, R. Schäafer, L. Schultz, and R. Mattheis, Phys. Rev. B **78**, 094419 (2008).